NeuroImage 172 (2018) 492–505

Contents lists available at ScienceDirect

NeuroImage

journal homepage: www.elsevier.com/locate/neuroimage

The dynamics of human cognition: Increasing global integration coupled with decreasing segregation found using iEEG

Josephine Cruzat [a,*], Gustavo Deco [a,b,c,d], Adrià Tauste-Campo [a,e], Alessandro Principe [e], Albert Costa [a,b], Morten L. Kringelbach [f,g,h], Rodrigo Rocamora [e]

[a] Center for Brain and Cognition, Department of Information and Communication Technologies, Universitat Pompeu Fabra, Ramon Trias Fargas 25-27, 08005, Barcelona, Spain
[b] Institució Catalana de la Recerca i Estudis Avançats (ICREA), Barcelona, Spain
[c] Department of Neuropsychology, Max Planck Institute for Human Cognitive and Brain Sciences, 04103, Leipzig, Germany
[d] School of Psychological Sciences, Monash University, Melbourne, Clayton, VIC, 3800, Australia
[e] Epilepsy Unit, Department of Neurology, IMIM Hospital del Mar, Universitat Pompeu Fabra, Passeig Marítim, 25, 08003, Barcelona, Spain
[f] Department of Psychiatry, University of Oxford, OX3 7JX, Oxford, UK
[g] Center for Music in the Brain (MIB), Department of Clinical Medicine, Aarhus University, Nørrebrogade 44, Building 10G, 8000, Aarhus, Denmark
[h] Institut d'études avancées de Paris, France

ARTICLE INFO

Keywords:
Segregation
Integration
CTC theory
Cognition
iEEG

ABSTRACT

Cognitive processing requires the ability to flexibly integrate and process information across large brain networks. How do brain networks dynamically reorganize to allow broad communication between many different brain regions in order to integrate information? We record neural activity from 12 epileptic patients using intracranial EEG while performing three cognitive tasks. We assess how the functional connectivity between different brain areas changes to facilitate communication across them. At the topological level, this facilitation is characterized by measures of integration and segregation. Across all patients, we found significant increases in integration and decreases in segregation during cognitive processing, especially in the gamma band (50–90 Hz). We also found higher levels of global synchronization and functional connectivity during task execution, again particularly in the gamma band. More importantly, functional connectivity modulations were not caused by changes in the level of the underlying oscillations. Instead, these modulations were caused by a rearrangement of the mutual synchronization between the different nodes as proposed by the "Communication Through Coherence" Theory.

Introduction

Intracranial electroencephalography (iEEG) recordings from the human brain provide a unique opportunity to study cognitive functions measuring neural activity at the mesoscopic level. Beyond the high temporal resolution intrinsic to iEEG measurements, this technique also allows higher levels of spatial resolution and enhanced signal-to-noise ratio (Engel et al., 2005; Lachaux et al., 2003). These advantages have led scientists to use the technique (Lachaux et al., 2012) to study several cognitive processes such as attention (Musch et al., 2014), visual perception (Ossandon et al., 2012; Bertrand et al., 2014), language (Sahin et al., 2009; Chan et al., 2011; Hamame et al., 2014), memory (Kucewicz et al., 2014; Greenberg et al., 2015; Haque et al., 2015), decision making (Perez et al., 2015), emotion (Murray et al., 2014; Boucher et al., 2015) and consciousness (Gaillard et al., 2009). Most of this research has attempted to assign functions to specific local brain areas by correlating task-performance with measurements of neural activity - see also recent coherence network studies (Kingyon et al., 2015; Zheng et al., 2017; Mercier et al., 2015). Furthermore, most studies using iEEG have focused mainly on single-electrodes analysis, using predominantly event-related potentials (Lachaux et al., 2012) or spectral analysis (Kahana, 2006). Here, we take a different perspective. Instead of focusing on single electrodes, we assess changes in functional connectivity analysing all the implanted electrodes.

In contrast to the regional view of brain function, growing evidence reveals that human cognition relies on the flexible integration of information widely distributed across different brain regions (Bressler and Menon, 2010; Deco et al., 2015; De Vico Fallani et al., 2008; Wang et al., 2015; Kitzbichler et al., 2011; Palva et al., 2010; Valencia et al., 2008; Bassett et al., 2011; Chai et al., 2016; Ekman et al., 2012; Kinnison et al.,

* Corresponding author.
E-mail address: josephine.cruzat@upf.edu (J. Cruzat).

https://doi.org/10.1016/j.neuroimage.2018.01.064
Received 18 September 2017; Accepted 25 January 2018
Available online 6 February 2018

Table 1
Demographic and clinical characteristics of each patient.

Patient	Gender	Age (years)	Epileptogenic zone laterality	Seizure onset zone	Implanted Regions	N° of electrodes implanted	N° unipolar channels	N° of bipolar channels for analysis
A	Male	38	Left	Mesial temporal and amygdala	L (F-T-I-P)	8	85	76
B	Male	21	Left	Anterior temporal	L (F-T-I-P-O) & R (F-T)	15	125	95
C	Male	44	Right	Anterior temporal	L (T) & R (F-T-P)	12	125	104
D	Male	44	Right	Temporo-parietal	L (T) & R (F-T-I-P)	16	127	101
E	Female	43	Left	Anterior medial temporal	L (F-T-I-P-O)	11	127	112
F	Male	25	Right	Temporo-parieto occipital	R (F-T-I-P-O)	14	127	105
G	Male	23	Left	Temporal	L (F-T-I-P)	13	125	102
H	Female	43	Left	Posterior Temporal	L (F-T-I-P)	14	125	103
I	Male	44	Left	Mesial Temporal	L (F-T-I-P)	12	123	105
J	Female	46	Left	Anterior medial temporal	L (F-T-I-P-O)	11	124	107
K	Male	43	Left	Mesial Temporal	L (F-T-P)	9	103	94
L	Male	23	Right	Anterior temporal	R (F-T-P)	15	125	96

R: Right; L: Left; F: Frontal; T: Temporal; P: Parietal; O: Occipital; I: Insula.

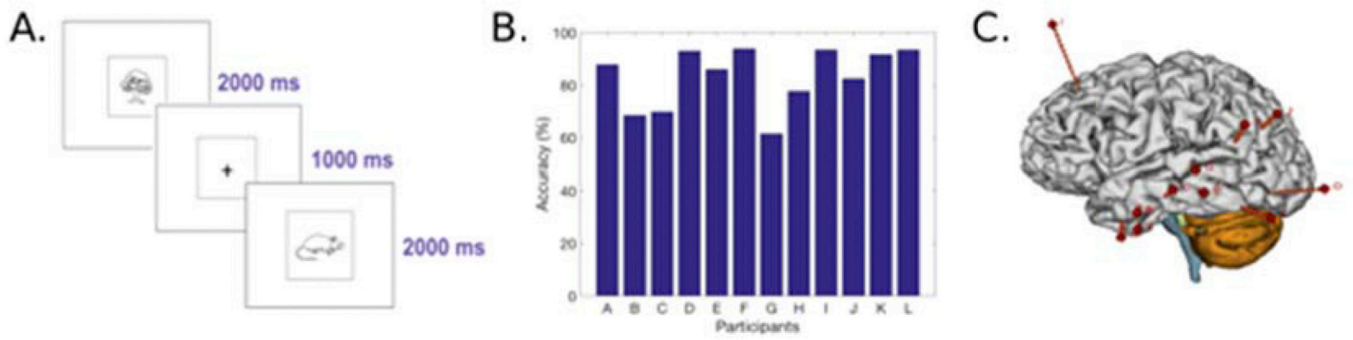

Fig. 1. Paradigm, behavioural performance and implantation scheme. A) Schematic example of the experimental paradigm of the picture-naming task. After an interval of 1000 ms for preparation, each target picture was presented and remained on the screen for 2000 ms. B) Picture naming accuracy for each patient. On average, patients achieved 83.2 ± 11.3% accuracy on test items (N = 228). C) Example of the intracerebral implantation scheme for iEEG recordings in patient E. Eleven electrodes were implanted in the left hemisphere.

2012; Wang et al., 2016). In these studies, cognitive processing increases the global integration of information across neural networks, while at the same time leads to a decrease in their modularity (Kitzbichler et al., 2011; Ekman et al., 2012; Kinnison et al., 2012; Bola and Sabel, 2015; Vatansever et al., 2015; Godwin et al., 2015; Liang et al., 2016). Although some iEEG studies have observed increased synchronization by task demands (Gaillard et al., 2009; Becher et al., 2015; Axmacher et al., 2008), no one has assessed integration and segregation dynamics. Furthermore, limited knowledge is available regarding the mechanisms that underlie changes in integration/segregation associated with cognitive processing.

The "Communication Through Coherence" (CTC) theory states that the communication between different neuronal populations could be modulated by the synchronization between them (Deco and Kringelbach, 2016). Indeed, two populations of neurons may communicate most effectively when they are coherent, i.e. when their excitability level is coordinated in time. The CTC theory suggests that effective connections in a network can be shaped through phase relations, more specifically through gamma- and beta-band (30–90 Hz) synchronization, as reported experimentally (Fries, 2005, 2009, 2015). Thus, oscillations are proposed to dynamically shape the computational role of different neuronal groups linked through static structural connectivity. Several empirical studies support task-induced changes in synchronization at the level of individual regions during selective attention (Womelsdorf et al., 2006), working memory (Howard et al., 2003), and motor control (Ball et al., 2008). Moreover, such task-induced changes in synchronization have been observed between distant cortical regions during working memory (Jones and Wilson, 2005), long-term memory encoding (Fell et al., 2001), visual attention (Gregoriou et al., 2009), and sensorimotor integration (Roelfsema et al., 1997).

Here, we explore how cognitive processing modulates the level of integration and segregation of information in human brain networks (Deco et al., 2015), and how this is related to CTC theory. To do so, we recorded iEEG data from depth electrodes stereotactically implanted for pre-surgical diagnosis in 12 epileptic patients performing three different cognitive tasks. The iEEG electrodes used a stereo-electroencephalography (SEEG) implantation methodology and covered broad brain regions including cortical as well as subcortical regions. Hence, we were able to assess global changes in a broad brain network. Furthermore, we also assessed how integration and segregation relate to synchronization rather than to the oscillations level (amplitude). Finally, we would like to emphasize that our claims about the modulation of integration/segregation and the validity of CTC theory are global, since they are independent from the location of the electrodes (i.e. node location, which was different for each patient) and type of cognitive processing (three different cognitive tasks were used).

Materials and methods

Ethics statement

The Clinical Research Ethical Committee of the Municipal Institute of Health Care (CEIC-IMAS) approved this study. Following the Declaration

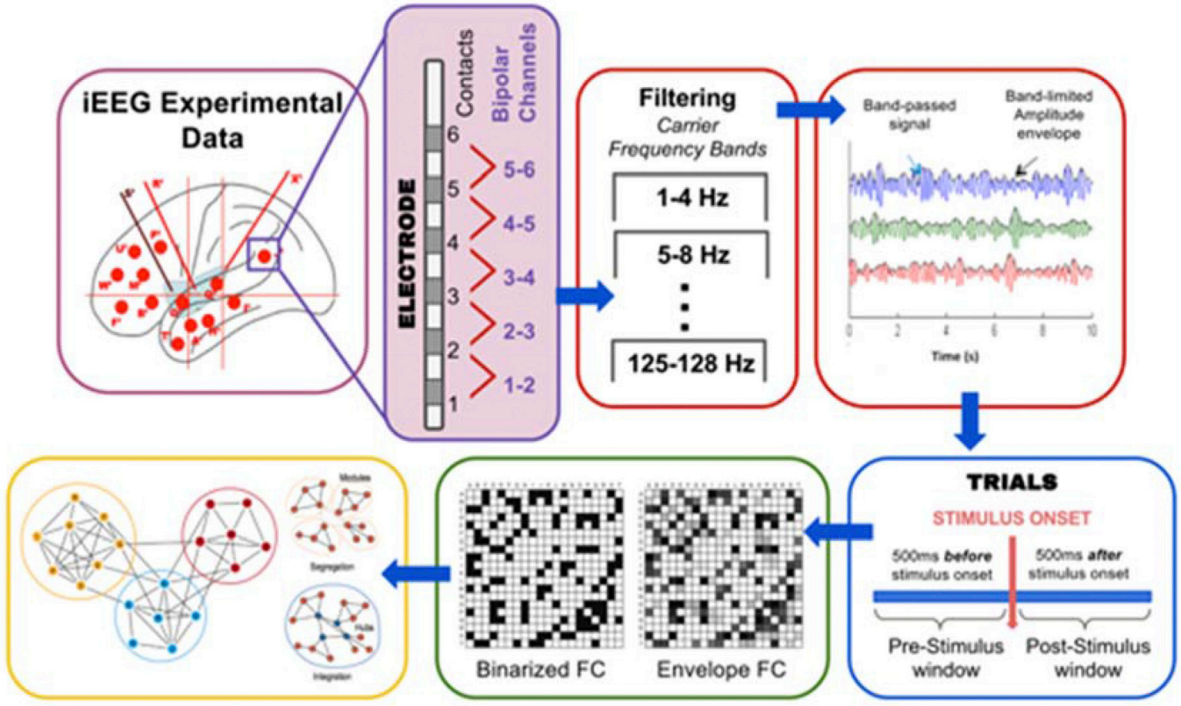

Fig. 2. Data processing flow chart. The iEEG data is recorded from 85 up to 127 unipolar channels on each patient. The bipolar montage is constituted offline by subtracting the neural activity recorded by neighbouring contacts within the same electrode array. The data is first band-pass filtered at 1–150 Hz, and further band-pass filtered into narrow frequency bands [$f_{carrier}$-2, $f_{carrier}$+2 Hz] (we consider here carrier frequencies $f_{carrier}$ = 1–130 Hz in steps of 4 Hz). By the Hilbert transform the corresponding amplitude envelopes are computed to further compute the envelope FC matrix. The continuous data is segmented into windows of −500 to 0 ms (pre-stimulus window) and 0–500 ms (post-stimulus window), around stimulus presentation. In order to characterize the organization of the network under both windows, we used the integration and segregation measures of global brain function.

of Helsinki, patients were informed about the procedure and they gave their written consent before the experiment.

Participants

Twelve participants (N = 12) (3 women; all right-handed; mean age 36.4 ± 10.1 years-old), evaluated for presurgical diagnosis in the Epilepsy Monitoring Unit of the Hospital del Mar (Barcelona, Spain), participated in the study. All patients were stereotactically implanted with depth electrodes for invasive presurgical diagnosis using a stereotactic ROSA robotic device (Medtech, France). The location of the electrodes was established only for clinical reasons using a SEEG approach. The implantation schemas were similar between all patients given that they were all under investigation for temporal lobe epilepsy. The number of electrodes used varied among 8 to 16 for patient with 5–15 contacts each (diameter: 0.8 mm; contacts 2 mm long, 1.5 mm apart) (DixiMédical, France). All patients underwent an extensive neuropsychological evaluation and had normal or corrected-to-normal vision. They were within the normal range of education having completed from primary to high academic level. Table 1 summarizes personal data, pathological information and overview of implanted electrodes for each patient. Since we aim to study the network dynamics supporting cognitive processes under normal circumstances, patients were assessed in absence of pharmacological treatment. They were tested at least three days after the last administration of the drug.

Cognitive tasks

Picture-naming task

Participants were asked to name aloud in Spanish, as fast and accurately as possible, 228 pictures presented in three different blocks. Pictures were black & white line drawings of familiar objects from a wide range of semantic categories selected from the Snodgrass and Vanderwart (1980) set. Each picture appeared once centrally and sequentially on the computer screen in a pseudo-random order for 2000 ms followed by a fixation cross for 1000 ms (see Fig. 1).

Size-judgement task

Participants were instructed to indicate via button press if the presented Spanish word represented an object larger than one-foot box in any dimension. Word stimuli were 68 items from two different categories: animals and man-made objects. Half of the words in each category represented objects larger than one foot. Words were auditory-presented through the computer speakers. Each word was presented sequentially in a pseudo-random order followed by an inter-trial lapse of 3500 ms.

Lexical-decision task

Participants were instructed to indicate whether the letter string presented in each trial written on a computer screen was a real word (e.g. run, table) or a pseudo word (e.g. lun, tible). We included four types of real words: motion verbs (e.g. run), static verbs (e.g. think), concrete nouns (e.g. table) and abstract nouns (e.g. theory). The task included a total of 150 trials. Each word was presented once centrally and sequentially on the computer screen in a pseudo-random order for 2000 ms followed by a fixation cross for 1000 ms.

The three tasks had different stimulus presentation modality. This allowed us to assess neural activity elicited when retrieving conceptual knowledge from a lexical form, from an object depicting a concept and from a written lexical form.

Stimulus were presented using the software Sketchbook Processing 2.2.1 (Programming Software, 2001 https://processing.org/) on a laptop computer at an approximate size of 5 degrees of visual angle. For the picture-naming task, the experimenter transcribed the responses and provided an accuracy score. For the size-judgement and lexical-decision

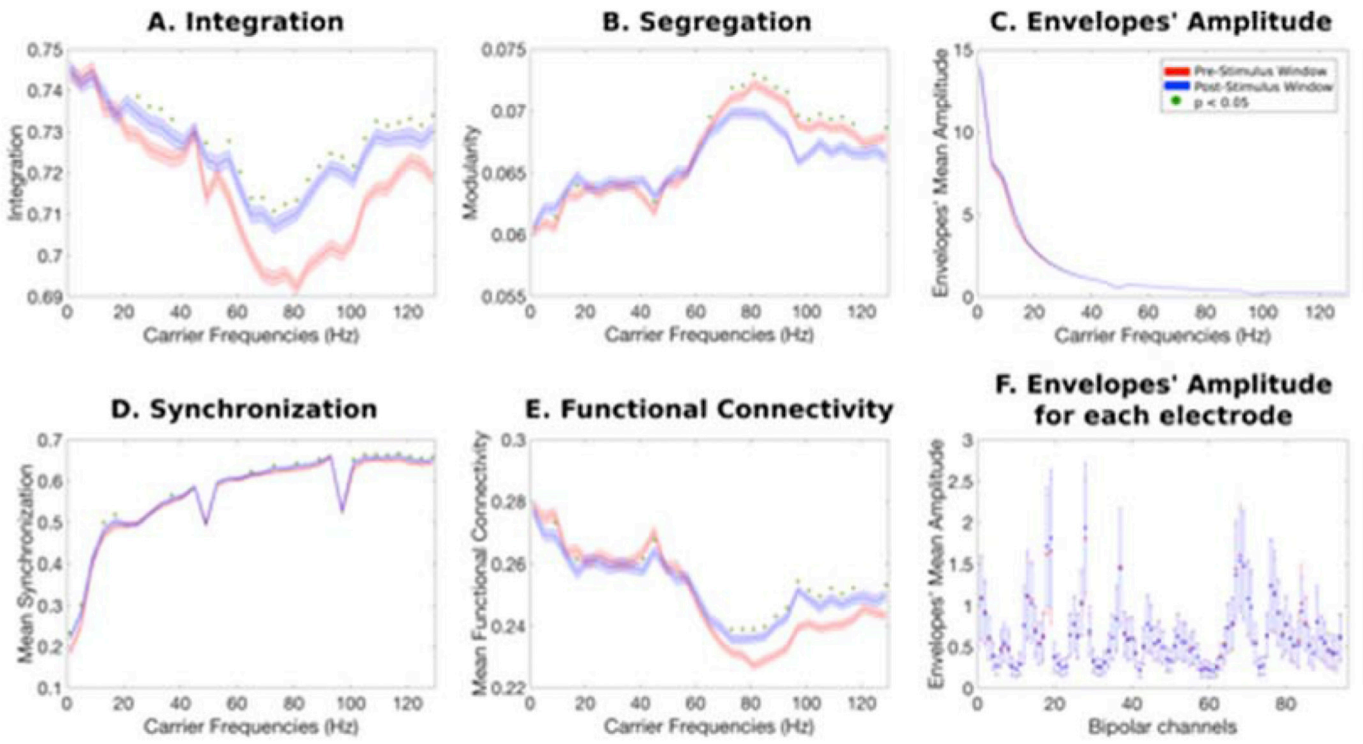

Fig. 3. Results analysis patient K for the picture-naming task. Panel A shows a significant increase in the integration during cognitive processing. The greatest effect is observed in the gamma range (50–90 Hz). The red line corresponds to pre-stimulus window, the blue line corresponds to post-stimulus window, the shaded error regions reflect the standard deviation across trials and green dots indicate a statistical significance of $p < 0.05$ ($N = 1000$). Complementary to the integration, panel B shows a decrease of the modularity in the same frequency range. Panel C shows that there are no iEEG oscillations amplitude changes in any frequency induced by the stimulus (both curves are strongly overlapped). This result indicates that the increase of integration and decrease of modularity could not be explained by changes in the oscillations amplitude. Panel D shows an increase of mean synchronization over a broad range of frequencies that is more conspicuous in the gamma band range (50–90 Hz) for the post-stimulus window. Panel E shows that the functional connectivity behaves coherently with the other results, as it increases as a function of the stimulus presentation particularly in the gamma range. Panel F plots the amplitude of the oscillations envelope at 60 Hz for each bipolar channel and pre- and post-stimulus window. There are no noticeable modulations across single bipolar channels between pre- and post-stimulus window. Note that the sharp peaks at 50 and 100 Hz are due to the power-line noise created by the electrical power.

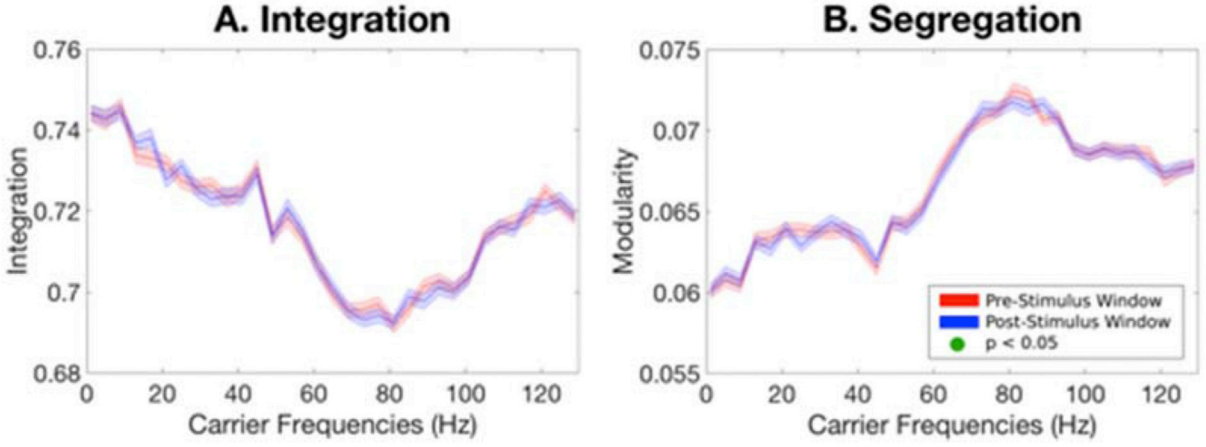

Fig. 4. Inter pre-stimulus presentation window comparison for the picture-naming task. Panel A shows the result of the measure of Integration, and panel B shows the result of the measure of Segregation, when contrasting half of pre-stimulus trials against the other half. There is no modulation of any of the two measures before stimulus presentation. The red line corresponds to 50% of pre-stimulus windows; blue line corresponds to the other 50% of pre-stimulus window. The shaded error regions reflect the standard deviation across trials. Green dots indicate a statistical significance of $P < 0.05$ ($N = 1000$).

task, responses were collected through keyboard input and response times recorded and timed in milliseconds. An electronic processor "Arduino, UNO" was used to connect and synchronize both hardware; the XLTEK system with the computer (MacBook Pro). The application interfaced with an Arduino board that in turn was connected to the EEG amplifier, and at each trial a signal was sent through the Arduino to the EEG.

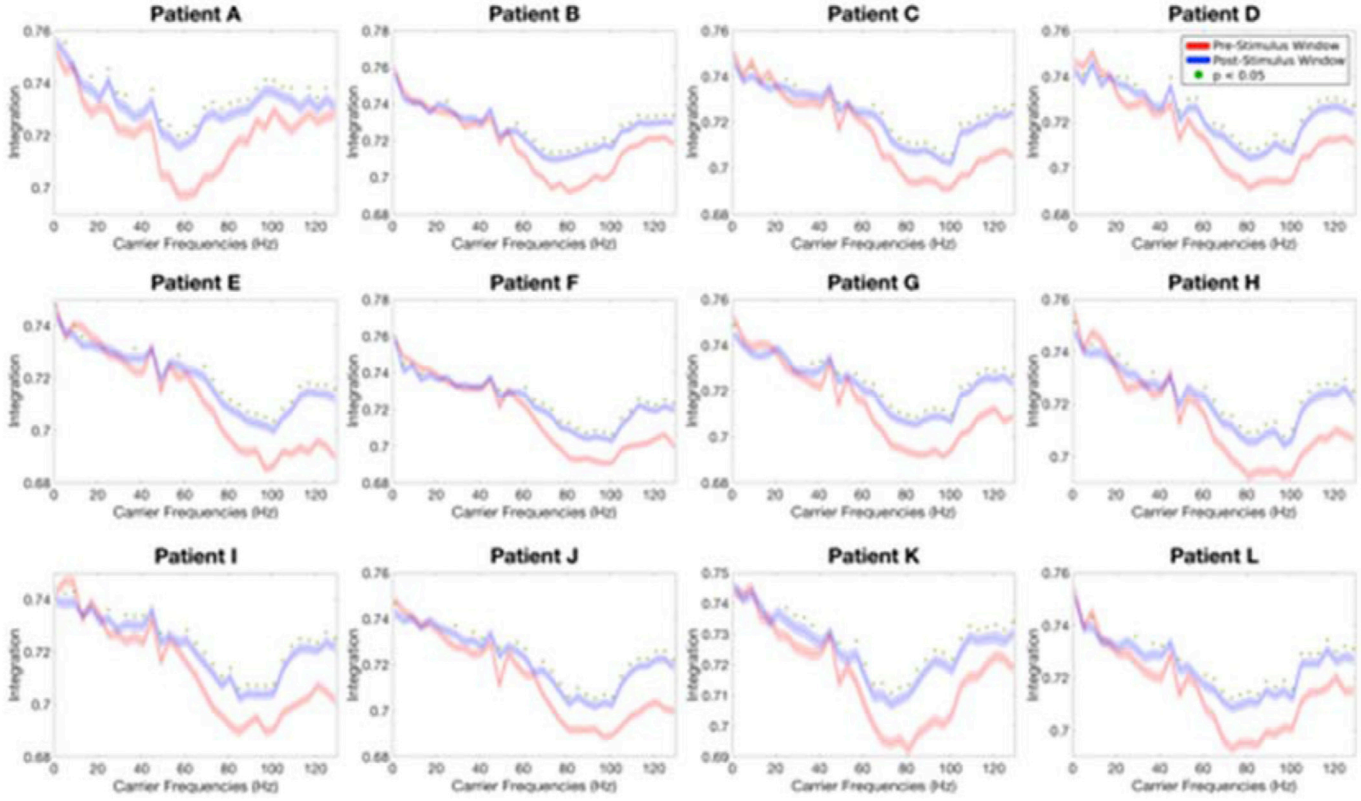

Fig. 5. Integration measure results for each patient. The panels show the results for every single patient for the picture-naming task. As can be seen, despite the heterogeneity of the recording sites, all patients show a significant increase of the integration related to cognitive processing. For all patients, the greatest effect was found in the gamma range. The red line corresponds to pre-stimulus window, blue line corresponds to task condition, the shaded error regions reflect the standard deviation across trials and green dots indicates a statistical significance of $p < 0.05$ ($N = 1000$).

iEEG data acquisition and pre-processing

Neurophysiological responses were registered by the iEEG system from deep multichannel electrodes (DIXI Microtechniques, Besançon, France). On average, each patient had 13 ± 2 electrodes implanted (range 8–16) with a total of 120±13 recording contacts (range 85–127). The data were acquired continuously by the Neuroworks XLTEK system (version 6.3.0, build 636) at 32 kHz with a headbox of 128 channels recorded at a sampling frequency of 500 Hz. For our analysis, we considered all channels placed in both cortex and subcortical structures. Channels placed in white matter or misplaced were disregarded.

A bipolar montage was constituted offline to increase spatial resolution by removing any confounds from the common reference signal (Lachaux et al., 2003; Jerbi et al., 2009). Bipolar signals were derived by differentiating neighbouring electrode pairs of recorded and not rejected consecutive channels within the same electrode array (Lachaux et al., 2012; Boucher et al., 2015; Gaillard et al., 2009; Burke et al., 2013). The continuous iEEG data was first high-pass filtered at 1 Hz and low-pass filtered at 150 Hz. To remove common line contamination an extra notch filter was applied at 50 and 100 Hz. In order to have specific spectral information, we analysed the spatio-temporal correlations of the Band Limited Power (BLP) at a given carrier frequency. This is a standard approach introduced in the context of MEG analysis (Brookes et al., 2011a). For that, at a given carrier frequency $f_{carrier}$ (we consider here $f_{carrier} = 1$–130 Hz in steps of 4 Hz) we band-pass filtered the signal within the narrow band [$f_{carrier}$-2, $f_{carrier}$+2 Hz] (we used the second order Butterworth filter) and computed the corresponding envelope using the Hilbert transform (Brookes et al., 2011b; Cabral et al., 2014). The Hilbert transform yields the associated analytical signals. The analytic signal represents a narrowband signal, s(t), in the time domain as a rotating vector with an instantaneous phase, φ(t), and an instantaneous amplitude, A(t), i.e., $s(t) = A(t)\cos(\varphi(t))$. The phase and the amplitude (envelope of that carrier frequency) are given by the argument and the module, respectively, of the complex signal z(t), given by $z(t) = s(t) + i.H[s(t)]$, where i is the imaginary unit and H[s(t)] is the Hilbert transform of s(t). We further consider only the slow components of the envelope A(t) by filtering the amplitudes again below 12 Hz (Nir et al., 2008). Finally, the slow component of the envelope of each brain node -which corresponds to each bipolar channel-at a given carrier frequency was used to calculate the envelope FC (see subsection below, Data Analysis).

In order to test another possible definition of integration, we also used the monopolar montage. Spatial resolution was increased by removing any confounds from the common reference signal for each time point. In this case, brain nodes correspond to each single monopolar channel.

Data analysis

Envelope functional connectivity (FC)

For the three tasks, all trials were considered. The data was segmented into two windows around stimulus presentation: the first one spanning from −500 ms to 0 from the stimulus presentation (pre-stimulus window), and the second one from 0 to 500 ms from stimulus onset (post-stimulus windows). We defined an Envelope FC matrix of the continuous bipolar iEEG data for pre- and post-stimulus windows as a matrix of Pearson's correlations of the corresponding amplitude envelopes, i.e. the slow components of the BLP of iEEG signals at a given carrier frequency between two brain areas over the whole-time window for a given window (pre- and post-stimulus). Thus, the mean FC is specific for each narrow band frequency window.

Phase-lock matrix

For each time point we calculated the phase lock matrix describing

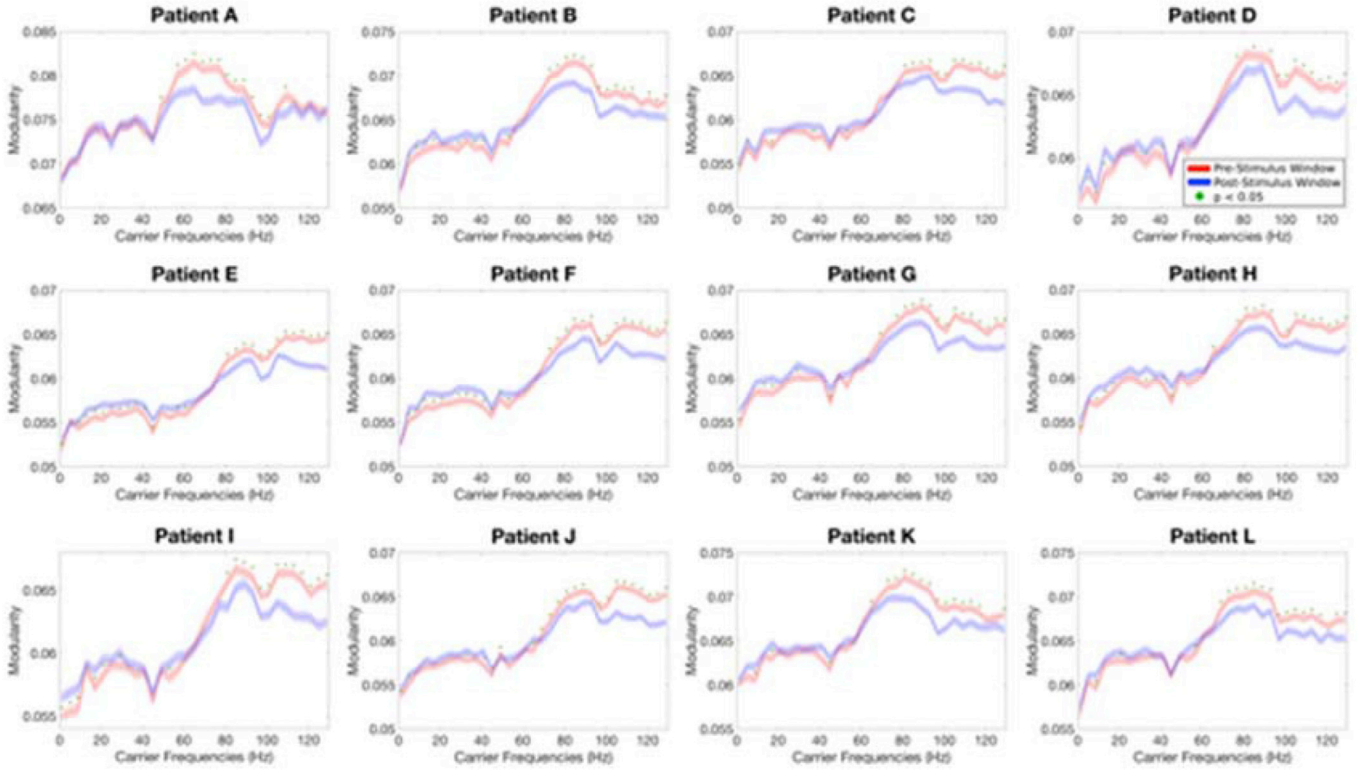

Fig. 6. Segregation measure results for each patient. The panels show the results of segregation (measured by the modularity) during pre- and post-stimulus window for the picture-naming task. For all patients, there is a significant decrease of the segregation during cognitive processing and the greatest effect can be seen in the gamma range (50–90 Hz). The red line corresponds to pre-stimulus window, blue line corresponds to post-stimulus window, the shaded error regions reflect the standard deviation across trials and green dots indicates a statistical significance of $p < 0.05$ ($N = 1000$).

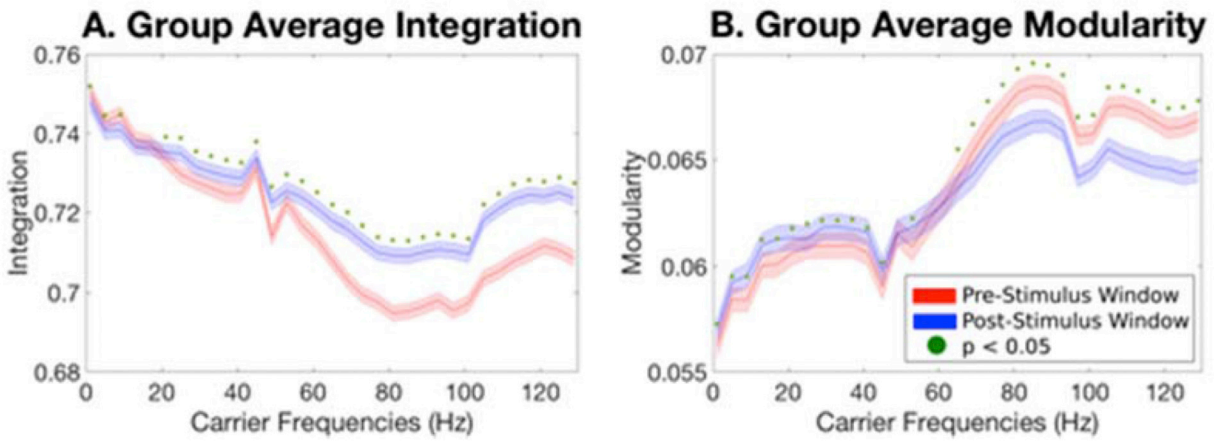

Fig. 7. Group Analysis. Panel A shows a significant increase in integration during cognitive processing for almost all frequencies, but with the greatest effect in the gamma range (60–100 Hz) as seen on each single subject. Complementary to the integration, panel B shows a decrease of the modularity which is more prominent in the high gamma range. The red line corresponds to pre-stimulus window, the blue line corresponds to post-stimulus window, the shaded error regions reflect the standard deviation across trials and green dots indicates a statistical significance of $p < 0.05$ ($N = 1000$).

the global state of synchronization across all network nodes using the bipolar montage. The elements of the phase-lock matrix are given by:

$$P_{ij}(t) = e^{-3|\varphi_i(t)-\varphi_j(t)|}$$

where $\varphi_i(t)$ is the extracted phase of node *i* at time *t* (at a given carrier frequency using the Hilbert transform as specified above). We used the phase-lock matrix at a specific single time point to calculate the integration as specified below.

Integration

We used the measure of integration introduced by Deco et al (2015) defined at the network level, to characterize the level of broadness of communication between regions across the whole brain. After filtering the data, we calculated the envelope FC for both, the pre- and post-stimulus windows. Then, we define *integration* as the size of the largest connected component in the FC matrix. That is, the number of nodes of the largest connected graph in the binarized FC matrix obtained after thresholding it. More specifically, for a given absolute threshold θ between 0 and 1 (scanning the whole range), the FC (using the criteria

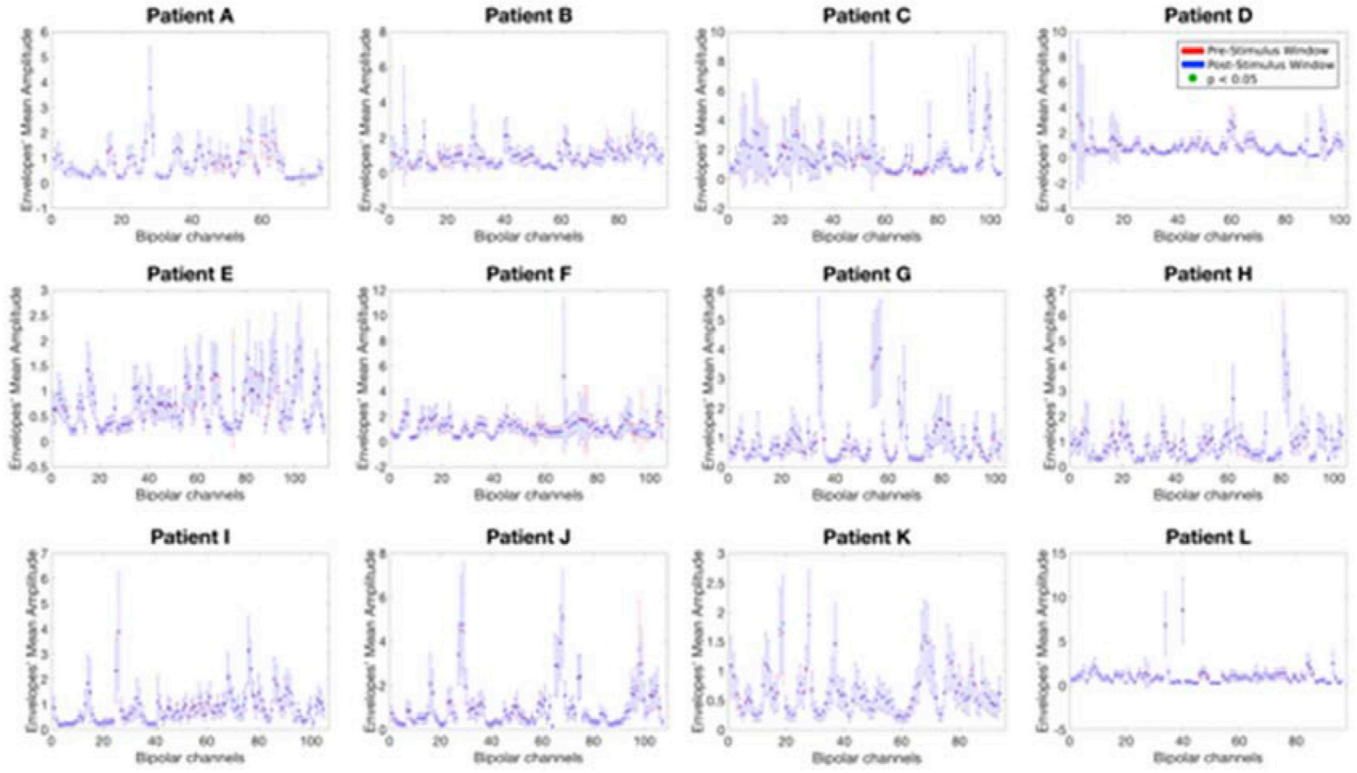

Fig. 8. Envelopes' Amplitude at 60 Hz across electrodes for each patient. The panels show the results of the mean amplitude and SD at 60 Hz for each bipolar channel and both pre- and post-stimulus window for the picture-naming task. For all patients, there is no noticeable modulation across single bipolar channels between pre- and post-stimulus windows. The red line corresponds to pre-stimulus window and the blue line corresponds to post-stimulus window. The shaded error regions reflect the standard deviation across trials. Note the strong overlap of both lines. Green dots indicate a statistical significance of $p < 0.05$ ($N = 1000$).

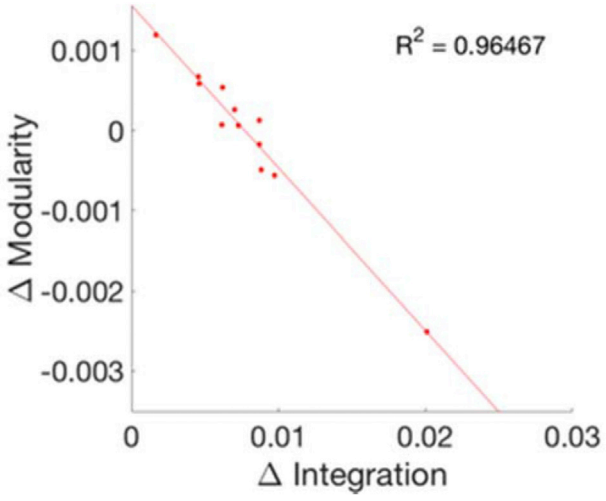

Fig. 9. Correlation between Integration and Segregation. The figure shows the coefficient of determination between the integration and segregation measures across patients ($N = 12$) at 60 Hz. The R^2 represents the proportion of variance explained by a linear model. Note that both measures are highly correlated.

$|FC_{ij}|<\theta$, i. e a value of 0 and 1 otherwise) is binarized and the largest subcomponent (see definition below) extracted as a measure of integration. To get a measure that is independent of the threshold, this curve is integrated in the range of thresholds between 0 and 1. The integration measure is then normalized by the maximal number of connected brain areas (i.e. all N areas) for each integration step and by the number of integration steps such that the maximal integration is normalized to 1.

Note, that the concept of integration is designed to account for the broadness of communication across the brain, and thus require considering positive and negative correlations as potentially establishing a communication link. Therefore, we took the absolute values of the FC correlations. In other words, we quantified the broadness of communication (measured by means of correlation) regardless of whether the correlation values were negative or positive.

In graph-theoretical terms, subcomponents are extracted from the undirected graph defined by the binarized matrix (which itself is considered as an adjacency matrix). More precisely, a subcomponent is a subgraph in which paths connect any two vertices to each other, and which connects to no additional vertices in the super-graph (Deco et al., 2015). A vertex *u* is said to be connected to a vertex *v* in a graph *G* if there is a path in *G* from *u* to *v*. The concepts of subgraph and super-graph are defined as following: Let *H* be a graph with vertex set *V(H)* and edge set *E(H)*, and similarly let *G* be a graph with vertex set *V(G)* and edge set *E(G)*. Then, we say that *H* is a subgraph of *G* if $V(H) \subseteq V(G)$ and $E(H) \subseteq E(G)$. In such a case, we also say that *G* is a super-graph of *H*.

Segregation

Complementary to the integration, we used the modularity (Rubinov and Sporns, 2011) as a measure of segregation. Following Rubinov and Sporns (2011), modularity is defined as a measure of the goodness with which a network is optimally partitioned into functional subgroups, i.e. a complete subdivision of the network into non-overlapping modules, and supported by densely connected network communities. We consider the modularity of our envelope FC matrix. This matrix contains positive and negative weights, namely the corresponding correlation between two nodes. The modularity measure we use is given by,

$$Q^{GJA} = \frac{1}{v^+ + v^-} \sum_{ij} \left[\left(w_{ij}^+ - e_{ij}^+ \right) - \left(w_{ij}^- - e_{ij}^- \right) \right] \delta_{M_i M_j}$$

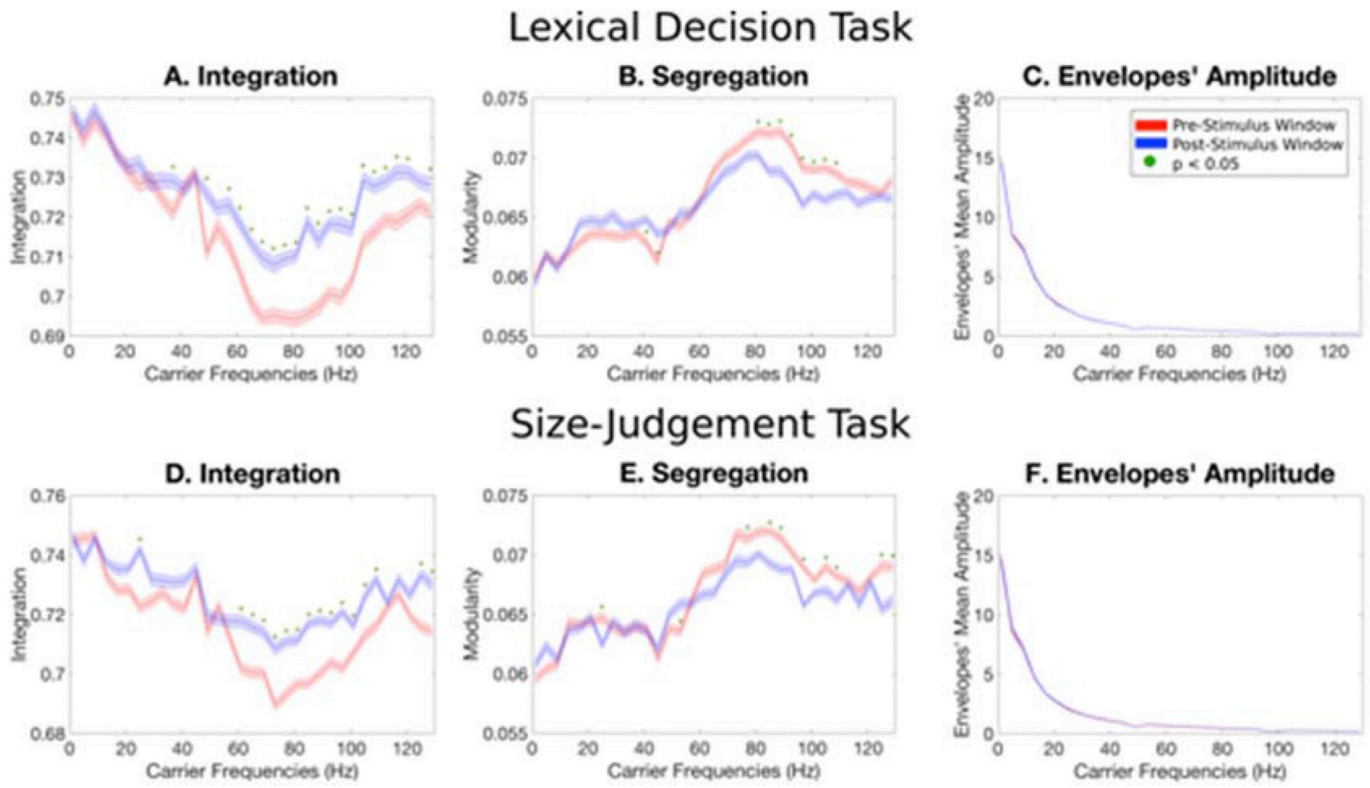

Fig. 10. Results analysis patient K for the Lexical Decision and Size-Judgement Task. Panels A and D shows a significant increase in the integration in the post-stimulus window (red line) compared to the post-stimulus window (blue line). The greatest effect is observed in the gamma range (50–90 Hz). The shaded error regions reflect the standard deviation across trials. Green dots indicate a statistical significance of $p < 0.05$ ($N = 1000$). Complementary to the integration measure, panels B and E shows a decrease of Segregation in the same frequency range. Panels C and F shows that there are no oscillations' envelope amplitude changes in any frequency induced by the stimulus (both curves are strongly overlapped). Note that the modulatory effect is almost the same for both tasks.

Where the total weight, $V^{\pm} = \sum_{ij} W_{ij}^{\pm}$, is the sum of all positive or negative connection weights (counted twice for each connection), being $w_{ij}^{\pm} \in (0,1]$ the weighted connection between nodes i and j. The chance-expected within-module connection weights $e_{ij}^{\pm} = \frac{s_i^{\pm} s_j^{\pm}}{v^{\pm}}$, where the strength of node i, $S_i^{\pm} = \sum_j W_{ij}^{\pm}$, is the sum of positive or negative connection weights of i. The delta $\delta_{MiMj} = 1$ when i and j are in the same module and $\delta_{MiMj} = 0$ otherwise (Newman, 2006). This definition is a generalisation of the standard measure of modularity for matrices with nonnegative weights, which is given by the average difference between present within-module connection weights $w_{ij}^{\pm}$ and chance-expected within-module connection weights $e_{ij}^{\pm}$. As mentioned above, here we consider both positively and negatively weighted connections (envelope FC matrix). The positively weighted connections represent correlated activation patterns and hence reinforce the placement of positively connected pairs of nodes in the same module. The negatively weighted connections represent anti-correlated activation patterns and reinforce the placement of negatively connected pairs of nodes in distinct modules. For a complete description see (Sporns, 2010).

Synchronization

We measure the global mean level of synchronization as the mean value of the Kuramoto order parameter across time. The Kuramoto order parameter is defined by following equation:

$$R(t) = \frac{\left| \sum_{k=1}^{n} e^{(i\varphi_k(t))} \right|}{n}$$

where $\varphi_k(t)$ is the instantaneous phase of each narrowband signal at node k at a given carrier frequency by using the Hilbert derived phases of the slow component of the Band Limited Power (BLP) signals. The Kuramoto order parameter measures the global level of synchronization of the n oscillating signals. Under complete independence, the *n* phases are uniformly distributed and thus *R* is nearly zero, whereas for $R = 1$ all phases are equal (full synchronization).

Permutation tests

To examine the reliability of the post-stimulus window modulation, frequency-dependent statistical significance was assessed using a non-parametric test with 1000 random permutations. The statistic test was chosen to be the median across the differences between post and pre-stimulus measures. Following Winkler et al (2014), we simulated the null hypothesis of no stimulus modulation at any post-stimulus windows by randomly permuting pre- and post-stimulus samples at each paired trial (group exchangeability hypothesis) and computing the test statistic. These surrogate values formed a reference distribution, against which we compared the original statistic value. The proportion of permutations in which surrogate values matched or exceeded the original statistic value determined the test p-value (P) to be compared with the significance level. We obtained a p-value for each frequency band and applied multiple comparisons corrections with the False Discovery Rate (FDR) level of 0.05 using the Benjamini-Hochberg method.

Results

We investigate how cognitive processing modulates the level of integration and segregation in human brain networks and how these modulations are related to the CTC theory. To do so, we exploited the high spatiotemporal resolution of intracranial electroencephalography (iEEG); a technique usually employed in pharmacologically resistant

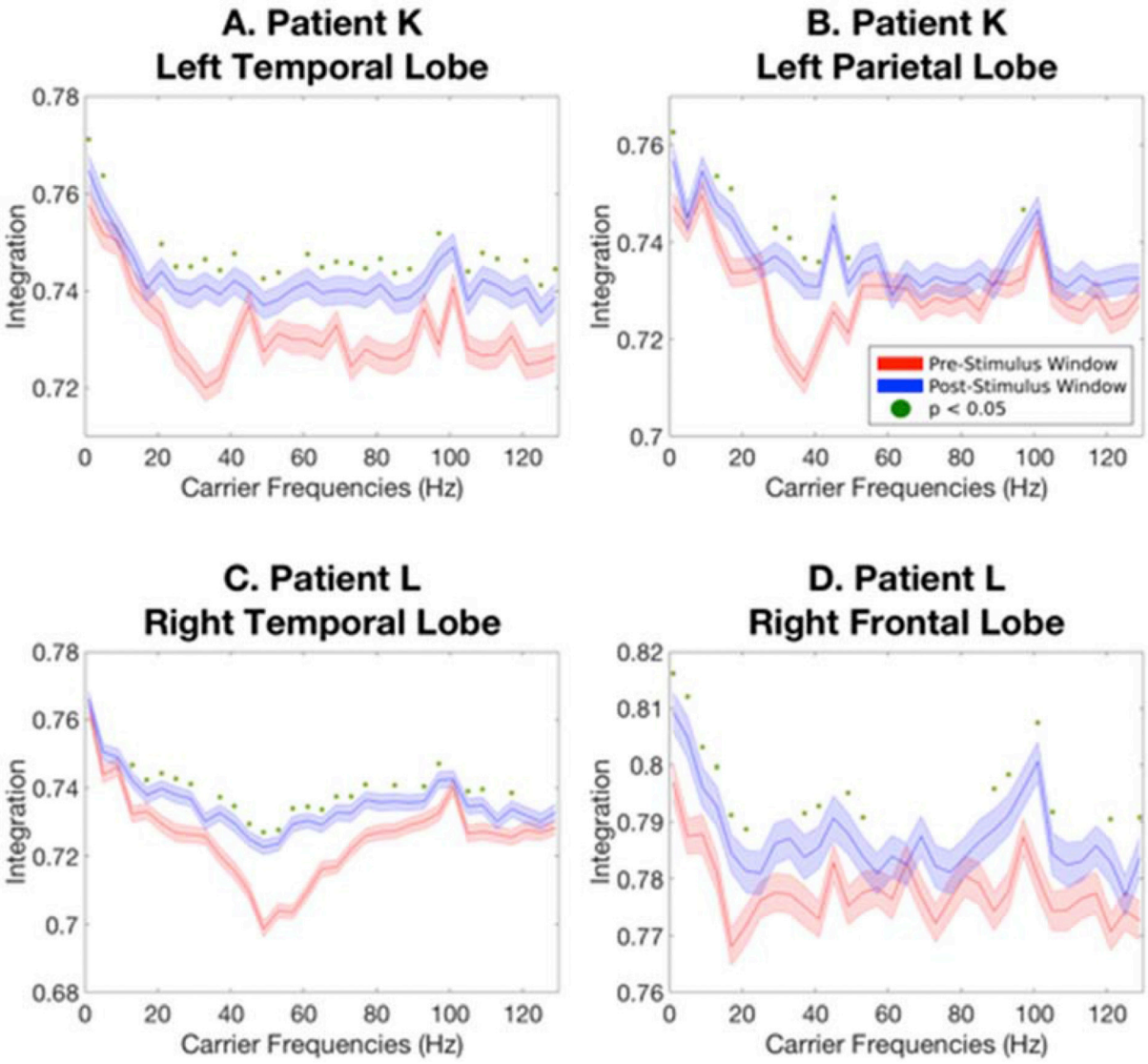

Fig. 11. Results of the analysis of sub-networks within frontal, temporal and parietal lobes for the Picture-naming task. The upper panels show a significant increase of the integration in the post-stimulus window (red line) compared to the post-stimulus window (blue line) in the left Temporal (A) and left Parietal (B) lobes for patient K. The greatest effect is observed in the gamma range (50–90 Hz). The shaded error regions reflect the standard deviation across trials. Green dots indicate a statistical significance of $p < 0.05$ ($N = 1000$). Panels (C) and (D) shows the results of the right temporal and Frontal lobes respectively, for patient L. The modulatory effect is seen in the whole range of frequencies.

epileptic patients who require brain mapping before surgery (Lachaux et al., 2012; Sperling, 1997; Serletis et al., 2014).

We recorded iEEG data in twelve patients while they were naming pictures in their native language (Spanish) (see Materials and Methods) (Fig. 1A). Naming accuracy was high ($83.2 \pm 11.3\%$) with an averaged response time of 1350 ± 306 ms (Fig. 1B). The task was used to drive the modulation of the underlying brain networks related to the integration of task-related information. For the large majority of people, language processing is supported by a widespread large-scale network distributed across frontal, temporal, parietal and occipital lobes in the dominant hemisphere (Chai et al., 2016; Ferstl et al., 2008; Price, 2000). Channels were placed in all lobes in both hemispheres, being most of them in the left frontal, temporal and parietal lobes (see an example of implantation scheme in Fig. 1C). All channel recordings from grey matter and subcortical structures were considered for the analysis.

After data pre-processing, we analysed the Band Limited Power (BLP) at a given carrier frequency ($f_{carrier}$) in order to have specific spectral information. We band-pass filtered the iEEG signals within the narrow band [$f_{carrier} - 2$, $f_{carrier} + 2$ Hz] and considered a range of $f_{carrier}$ starting from 1 to 130 Hz in steps of 4 Hz. We chose a bandwidth of 4 Hz because it provides a good trade-off between phase estimation accuracy and number of testable comparisons. In order to compute the envelope Functional Connectivity (FC), we further computed the Hilbert transform (Fig. 2).

To study functional network topology changes during task execution, we contrasted differences in brain activity in two time-windows: 500 ms before the stimulus was presented: *"pre-stimulus window"*, and 500 ms immediately after the stimulus was presented: *"post-stimulus window"* As speech production is associated with large motor activity, thus with a significant increase of integration, we focused our analysis in a time window far from the beginning of the motoric activity (response times were around 1350 ms and we recorded the first 500 ms). In order to characterize the organization of the network in both windows, we used the integration and segregation measures of global brain function (see Materials and Methods) characterizing the level of communication across the different nodes of the brain network. We tested the statistical significance of the network measure differences between pre-stimulus and post-stimulus using a non-parametric method (Winkler et al., 2014).

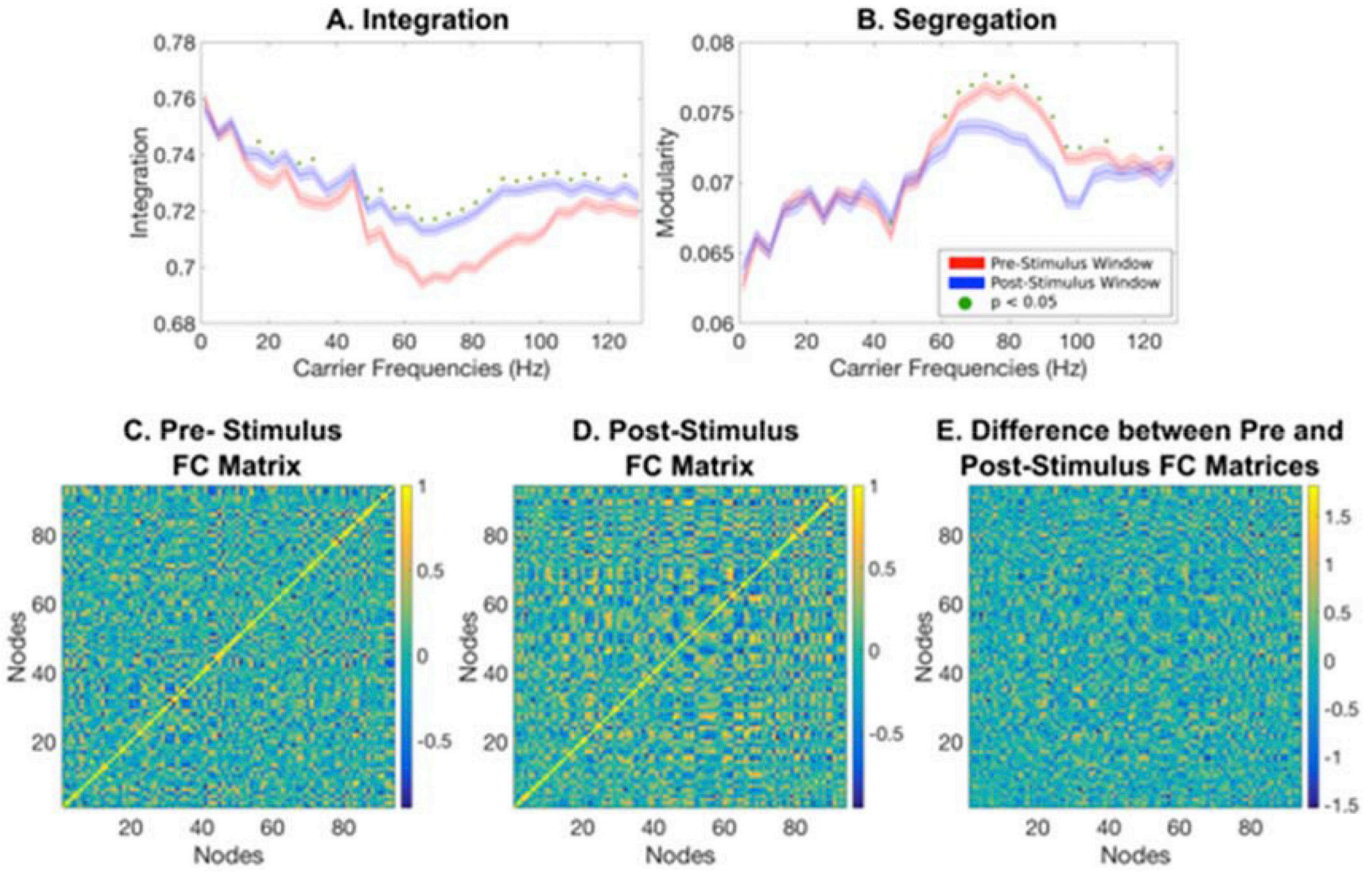

Fig. 12. Results analysis using the FC matrix based on the monopolar montage for Patient A. Panels A and B show the integration and segregation modulation during pre- and post-stimulus presentation, respectively, for the picture-naming task. The red line corresponds to pre-stimulus window, blue line corresponds to post-stimulus window. The shaded error regions reflect the standard deviation across trials and green dots indicate a statistical significance of $p < 0.05$ ($N = 1000$). Panels C and D shows the FC matrices computed for 60 Hz for the pre- and post-stimulus windows respectively. Panel E shows the difference between pre- and post-stimulus windows. The differences between both matrices (C and D, expressed on E), evidence the distributed character of the modulation across many different nodes.

Specifically, we characterized the null hypothesis using constrained permutations that preserved the trial grouping of the data at both time windows (Materials and Methods).

To illustrate the results, we first focus on the ones corresponding to a single patient (Fig. 3). The post-stimulus window as compared to the pre-stimulus one led to an increase in neural integration and to a decrease in neural segregation (Fig. 3A and B). For both indexes, the largest modulation appeared particularly in the gamma band, around 50–90 Hz ($p < 0.05$, $N = 1000$). Note that the concepts of integration and segregation are measures that, by definition, are calculated independently from each other but, at the same time, are highly correlated; when one increases the other consistently decreases. Thus, these results show that cognitive processing leads to an increase in neural integration and a decrease in neural segregation.

We further analyse the correlates of these modulations associated with the cognitive task. First, these modulations are not related to changes in oscillations' envelope amplitudes at any frequency (Fig. 3C). This is so both when looking at the mean amplitude of all electrodes and when evaluating the mean amplitude of each bipolar channel separately at 60 Hz (which corresponds to the maximal modulation of the integration measure) (Fig. 3F). Hence, changes in integration and segregation cannot be accounted by changes in oscillations' envelope amplitudes.

Second, the modulation of integration and segregation associated with the cognitive task was related to an increase in the global synchronization of cortical activity (measured using the Kuramoto Order Parameter). This increase was present over a broad range of frequencies, being the largest at the gamma range (50–90 Hz) (Fig. 3D).

Third, we assess whether integration and segregation were related to differences in Functional Connectivity (see Materials and Methods) between channels. This connectivity was calculated by considering the instant amplitude envelopes of all frequencies. Indeed, the Envelopes' Functional Connectivity is enhanced during task performance, in particular in the gamma range (50–90 Hz) (Fig. 3E).

When comparing two different time windows in which no task was performed, no changes in integration and segregation were found. Fig. 4a and b shows the lack of integration and segregation modulation when we contrasted the pre-stimulus windows of half the trials against the other half (same windowing as before, i.e. 500 ms before stimulus presentation). This result suggests that changes in these two measures are related to cognitive processing.

All together, these observations reveal that changes in integration and segregation (and their relationship) are likely related to a global increase of the connectivity, especially in the gamma band. Furthermore, changes in oscillations' envelope amplitudes cannot explain these phenomena. This pattern is consistent with the notion that communication between different brain networks is accomplished by means of the level of synchronization as posited by the *Communication Through Coherence Theory (CTC)* (Fries, 2005, 2015).

When looking at all patients, and despite the heterogeneity of the recording sites, the same pattern of modulation is observed for each individual as can be appreciated in Figs. 5 and 6, (Fig. 7 shows the group average data for both measures). Interestingly, in most of the patients, there is a consistent decrease of the segregation in the gamma band but with a slight increase of the segregation in the sub-gamma regime. This is

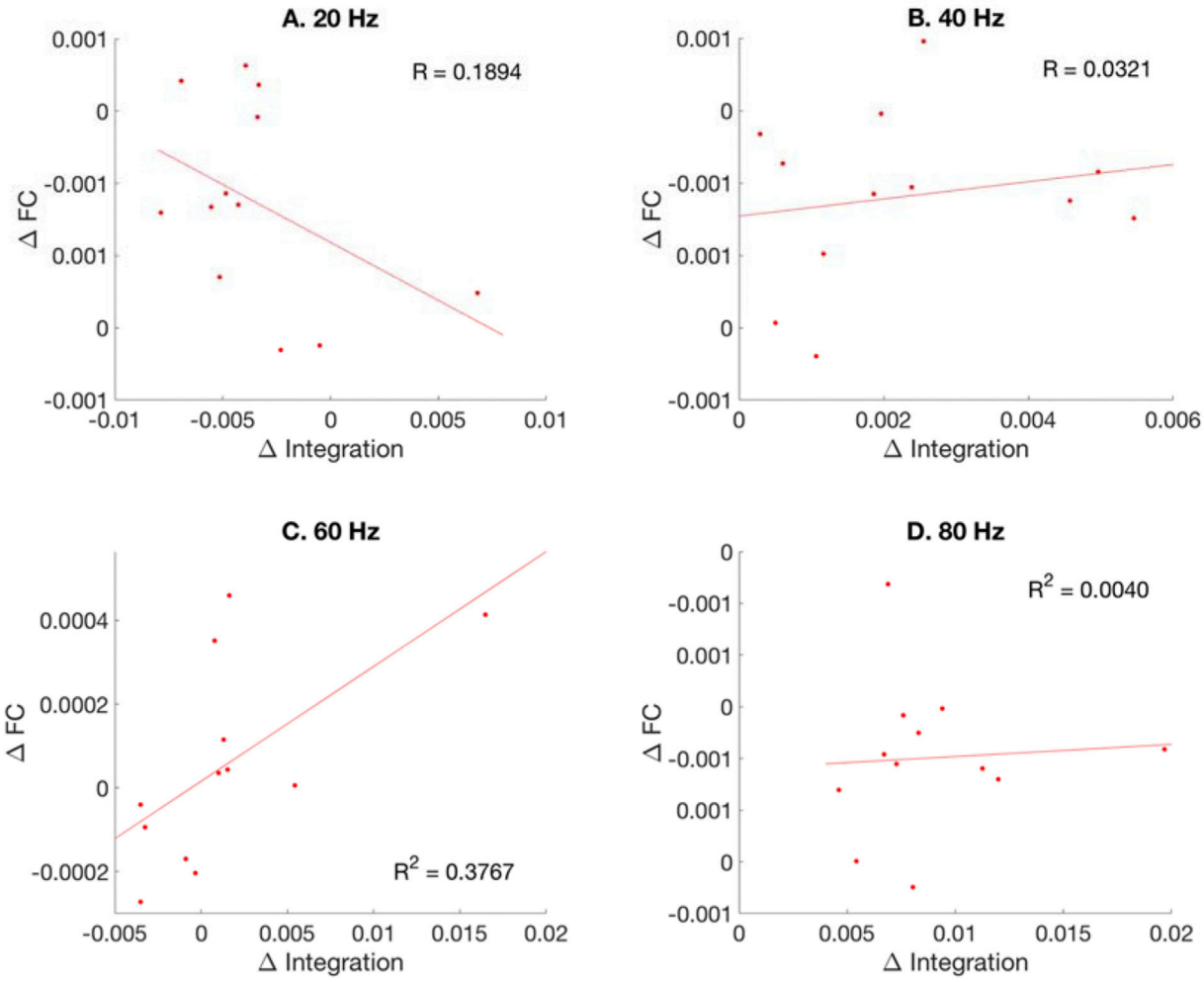

Fig. 13. Correlation between Integration and Functional Connectivity. The figure shows the coefficient of determination between the integration and the mean variance of the functional connectivity calculated at 20, 40, 60 and 80 Hz across the studied patients (N = 12) based on the monopolar montage. The R^2 represents the proportion of variance explained by a linear model. In all cases there is no correlation between both measures.

not observed for the integration measure. Furthermore, differences in oscillations' envelope amplitude at 60 Hz for each bipolar channel do not differ between pre- and post-stimulus windows (Fig. 8).

Importantly, the integration and segregation modulations calculated at 60 Hz were highly correlated (Fig. 9). Conversely, the network measures were independent of patient's performance (correlation coefficient of 0.0242, N = 12 patients).

These main results were robust since they were observed also in the other two tasks: a lexical decision task and a size judgement task (see Materials and Methods). Accuracy in both tasks was high (81.8 ± 5.1% and 88.7 ± 8.3% respectively) and response times for the lexical decision task was 1481 ± 398 ms and for the size judgement task 1008 ± 287 ms. A significant increase of the integration in the post-stimulus window was observed in the two tasks as shown for one patient (see Fig. 10). Furthermore, the largest modulation appears in the gamma band (around 50–90 Hz) for both measures, and no changes in the oscillation's envelope mean amplitude were observed.

The global nature of the integration is demonstrated by analysing different subnetworks independently. In two patients, we use the precise anatomical location of each electrode channel, and perform the integration analysis restricted to three specific subnetworks, namely the frontal, temporal and parietal. As shown in Fig. 11, even though the greatest modulations were found in both right and left temporal lobes, the parietal and frontal subnetworks were also modulated due to cognitive processing. This suggests that broadcasting of communication across the brain has a global nature.

Regarding technical issues, it is important to note that the results are independent on whether we used a bipolar or monopolar montage. We compared the new integration/segregation measurements with the more classical approach considering the pairwise changes in the FC between the post- and pre-stimulus windows (see Fig. 12 for a single patient). The results are consistent with the previous analysis and confirm the robustness of the findings. Fig. 12C and D shows the FC matrices calculated at 60 Hz for the pre-stimulus window and post-stimulus window respectively. The difference between both matrices demonstrate the distributed character of the modulation across many different nodes (Fig. 12E). Furthermore, this result supports the notion that the cognitive-driven global changes in integration and segregation are indeed not associated with any particular anatomical position inside the networks considered. Figure S1 in the Supplementary Materials shows the results for all patients.

Interestingly, the integration measure we use differs and complements the more classical measure of pairwise Functional Connectivity. As shown in Fig. 13, there is no correlation between the integration measure and the mean changes in the FC between the post- and pre-stimulus windows, for different frequencies in the gamma range.

Finally, we found that the modulation of integration is not solely driven by the stimulus's presentation, but it is persistently increasing after its onset. For this purpose, we extended the analysis of the integration measure by using the phase-lock matrix; a more explicit measure

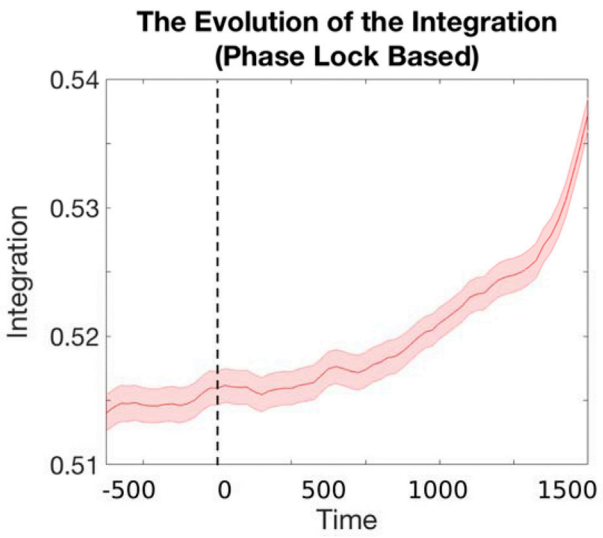

Fig. 14. Time evolution of the Integration measure for Patient K during the picture-naming task. The figure shows the integration measure calculated for the phase-lock matrix for every single time point for the whole period of time at 80 Hz. As seen, there is a monotonic increasing behaviour of the integration starting after the stimulus onset. The shaded error regions reflect the standard deviation across trials.

of communication according to CTC theory). The phase-lock matrix (see Materials and Methods) characterizes the global state of mutual synchronization between all pairs of network nodes at each single time point. Thus, with this matrix we are able to study the temporal evolution (in milliseconds) of the integration across time (see Fig. 14). This result was found in all three tasks.

Discussion

As a complex system, the human brain is organized into large-scale networks. In order to support cognitive functions, these networks need to flexibly adjust their functional connectivity to integrate relevant information towards a goal-directed behaviour (Bressler and Menon, 2010; Deco et al., 2015; Bola and Sabel, 2015). Traditionally, graph and information theoretical approaches have helped to characterize the global network connectivity in terms of *segregation* and *integration* (Deco et al., 2015; Tononi et al., 1994; Fox and Friston, 2012; Sporns, 2013). *Segregation* refers to the relative statistical independence of subsets of neurons or brain regions to compute information (Tononi et al., 1994; Sporns, 2013), while *integration* is a complementary concept quantifying the connectivity level across the whole-brain (Deco et al., 2015; Sporns, 2013). In particular, we used a measure of integration associated with the broadness of communication quantified by the length of the largest connected component of the functional connectivity across the whole brain (Deco et al., 2015), while for segregation we used the concept of modularity (Rubinov and Sporns, 2011).

We used intracranial EEG (iEEG) to record neural activity from 12 epileptic patients while they were performing three different cognitive tasks. We focus on how cognition modulates *global* functional network measurements, namely integration and segregation. We found a significant increase in integration and decrease in segregation during cognitive processing, especially in the gamma band (50–90 Hz). This was so for all patients and all tasks. Furthermore, these modulations were not associated with changes in the underlying level of oscillations. We also found significantly higher level of synchronization and functional connectivity during task processing, again particularly in the gamma band. This set of results suggest that changes in the broadness of communication across the entire extended network associated with cognitive processing could be due to a rearrangement of the coherence level between the nodes. This interpretation fits the predictions of the CTC theory extended to the whole-brain level (Deco and Kringelbach, 2016; Fries, 2005, 2015).

Our results extent the CTC hypothesis to the mesoscopic/macroscopic level by analysing the phases and correlations of the envelopes of the Band Limited Power as proposed by Deco & Kringelbach (Deco and Kringelbach, 2016). This is important since the CTC hypothesis posits that information is transmitted by synchronizing distinct neuronal populations, mainly in the gamma and beta-band (30–90 Hz) (Deco and Kringelbach, 2016). Note that the original CTC theory is based on a phase synchronization mechanism defined at the neuronal level.

Our findings are in line with previous neuroimaging studies showing increases of the integration across brain networks (Kitzbichler et al., 2011; Kinnison et al., 2012; Liang et al., 2016). There is also substantial agreement with studies using FC measurements that have revealed that local computations are likely to be highly segregated in spatially distributed network communities with clustered connectivity (Bassett et al., 2011; Ekman et al., 2012; Wang et al., 2016; Bola and Sabel, 2015; Power et al., 2011). Nevertheless, is important to note that our methodological approach is different from the classic FC approach and adds some critical information. In our results, the fact that integration and FC measures of band-limited power were not correlated suggest that the FC per se is not giving explicit information about how much the network is clustered. Indeed, one can have higher correlations but a lot of functional segregated clusters which in our measure is associated with low integration.

When analysing the performance, we did not find correlations between it and the modulation of the integration and segregation. Although we cannot presently elucidate the dynamical properties that leads to a better performance, the present findings suggest that the behavioural errors in our experiment are not captured in the time window we were looking at, or were not due to a failure at the global level of communication, but probably caused by failures at the local level of specific processing.

Interestingly, despite the global shift towards segregation in the gamma band during the task, we observed a slightly increase in segregation in the sub-gamma band. The decrease of the segregation in the gamma regime is expected and consistent with the increase of integration in the same regime which is putatively linked to increased stimuli/cognitive processing (Fries, 2015). Along the same lines, the increase of segregation in the sub-gamma bands could perhaps be associated with a disengagement of large slow resting networks. Future research is needed to understand this difference in sub-gamma bands.

It is important to remark that our results support the global nature of the functional large-scale network reorganization during cognitive processing. We demonstrate here that the pattern observed, that is an increase of the integration and a decrease of the segregation, appear in all patients irrespective of the heterogeneity of the implantation scheme. Moreover, this pattern is consistent when using a monopolar or bipolar montage. Further strengthening the results, we analysed three different cognitive tasks and we show that the main modulatory effect on the integration and segregation, and the validity of the CTC theory is independent of the particular cognitive processing. Thus, because of our global perspective, unlike many previous studies, we did not investigate the role of single channels in the different cognitive processes. Nevertheless, we are convinced that localising these electrodes in the human brain could lead to the discovery of interesting differences at the local spatial level and that this could be a very interesting goal for future investigations.

Our methodology and results open new avenues for further investigations. First, we need to understand how integration and segregation measures are modulated by task performance and/or task difficulty. Second, it is important to determine which specific brain areas, or local networks, show the highest degree of task-driven effective connectivity and therefore are mostly involved in information processing. Thus, future studies could greatly benefit from diffusion tensor imaging in two ways: to visualize and describe the precise connectivity between the electrodes

in the brain, as well as the basis of whole-brain models considering the connectivity and continuity of neural pathways in the patients.

Finally, we are aware of the potential methodological limitations of the iEEG technique with epileptic patients. First, these patients as compared to healthy controls, not only have epileptogenic neural activity, but may also have differences in the structural connectivity. Second, the lack of whole-brain coverage difficult to draw claims about the global network connectivity, given that restricted spatial coverage is simultaneously sampled. Still, and despite that the cognitive-driven changes observed on integration and segregation come from a reduced set of brain regions, we hypothesize that the effect is global across the whole brain. Thus, we predict that those changes should be consistently observed in fMRI and/or EEG/MEG experiments.

Conclusions

In this study, cognitive processing is associated with a global increase of integration and decrease of segregation, especially in the gamma band (50–90 Hz). These modulations probably reflect changes in how information is broadcasted in the brain. Going beyond our current knowledge on integration and segregation (see (Sporns and Betzel, 2016) for a review), we also show that such modulations were associated with a rearrangement of the band-limited functional connectivity between the different nodes and not with changes in the level of the underlying oscillations. This whole set of results is consistent with the "Communication Through Coherence" Theory.

Acknowledgements

The authors would like to thank all patients for their participation and the IMIM-Hospital del Mar Epilepsy Unit staff for their technical assistance in collecting the data. This work was supported by Gustavo Deco's ERC Advanced Grant: DYSTRUCTURE (n. 295129), from the European Union's Horizon 2020 research and innovation programme under grant agreement No. (HBP SGA1) and by the Spanish Research Project PSI2013-42091-P. M.L.K. is supported by the ERC Consolidator Grant CAREGIVING (n. 615539) and the Center for Music in the Brain, funded by the Danish National Research Foundation (DNRF117).

Appendix A. Supplementary data

Supplementary data related to this article can be found at https://doi.org/10.1016/j.neuroimage.2018.01.064.

References

Axmacher, N., et al., 2008. Interactions between medial temporal lobe, prefrontal cortex, and inferior temporal regions during visual working memory: a combined intracranial EEG and functional magnetic resonance imaging study. J. Neurosci. 28 (29), 7304–7312.
Ball, T., et al., 2008. Movement related activity in the high gamma range of the human EEG. Neuroimage 41 (2), 302–310.
Bassett, D.S., et al., 2011. Dynamic reconfiguration of human brain networks during learning. Proc. Natl. Acad. Sci. U. S. A. 108 (18), 7641–7646.
Becher, A.K., et al., 2015. Intracranial electroencephalography power and phase synchronization changes during monaural and binaural beat stimulation. Eur. J. Neurosci. 41 (2), 254–263.
Bertrand, J.A., et al., 2014. Recognizing an object from the sum of its parts: an intracranial study on alpha rhythms. J. Cogn. Neurosci. 26 (8), 1797–1805.
Bola, M., Sabel, B.A., 2015. Dynamic reorganization of brain functional networks during cognition. Neuroimage 114, 398–413.
Boucher, O., et al., 2015. Spatiotemporal dynamics of affective picture processing revealed by intracranial high-gamma modulations. Hum. Brain Mapp. 36 (1), 16–28.
Bressler, S.L., Menon, V., 2010. Large-scale brain networks in cognition: emerging methods and principles. Trend. Cogn. Sci. 14 (6), 277–290.
Brookes, M.J., et al., 2011. Investigating the electrophysiological basis of resting state networks using magnetoencephalography. Proc. Natl. Acad. Sci. U. S. A. 108 (40), 16783–16788.
Brookes, M.J., et al., 2011. Measuring functional connectivity using MEG: methodology and comparison with fcMRI. Neuroimage 56 (3), 1082–1104.
Burke, J.F., et al., 2013. Synchronous and asynchronous theta and gamma activity during episodic memory formation. J. Neurosci. 33 (1), 292–304.
Cabral, J., et al., 2014. Exploring mechanisms of spontaneous functional connectivity in MEG: how delayed network interactions lead to structured amplitude envelopes of band-pass filtered oscillations. Neuroimage 90, 423–435.
Chai, L.R., et al., 2016. Functional network dynamics of the language system. Cerebr. Cortex 26 (11), 4148–4159.
Chan, A.M., et al., 2011. First-pass selectivity for semantic categories in human anteroventral temporal lobe. J. Neurosci. 31 (49), 18119–18129.
De Vico Fallani, F., et al., 2008. Brain network analysis from high-resolution EEG recordings by the application of theoretical graph indexes. IEEE Trans. Neural Syst. Rehabil. Eng. 16 (5), 442–452.
Deco, G., Kringelbach, M.L., 2016. Metastability and coherence: extending the communication through coherence hypothesis using a whole-brain computational perspective. Trends Neurosci. 39 (3), 125–135.
Deco, G., et al., 2015. Rethinking segregation and integration: contributions of whole-brain modelling. Nat. Rev. Neurosci. 16 (7), 430–439.
Ekman, M., et al., 2012. Predicting errors from reconfiguration patterns in human brain networks. Proc. Natl. Acad. Sci. U. S. A. 109 (41), 16714–16719.
Engel, A.K., et al., 2005. Invasive recordings from the human brain: clinical insights and beyond. Nat. Rev. Neurosci. 6 (1), 35–47.
Fell, J., et al., 2001. Human memory formation is accompanied by rhinal-hippocampal coupling and decoupling. Nat. Neurosci. 4 (12), 1259–1264.
Ferstl, E.C., et al., 2008. The extended language network: a meta-analysis of neuroimaging studies on text comprehension. Hum. Brain Mapp. 29 (5), 581–593.
Fox, P.T., Friston, K.J., 2012. Distributed processing; distributed functions? Neuroimage 61 (2), 407–426.
Fries, P., 2005. A mechanism for cognitive dynamics: neuronal communication through neuronal coherence. Trend. Cogn. Sci. 9 (10), 474–480.
Fries, P., 2009. Neuronal gamma-band synchronization as a fundamental process in cortical computation. Annu. Rev. Neurosci. 32, 209–224.
Fries, P., 2015. Rhythms for cognition: communication through coherence. Neuron 88 (1), 220–235.
Gaillard, R., et al., 2009. Converging intracranial markers of conscious access. PLoS Biol. 7 (3), e61.
Godwin, D., Barry, R.L., Marois, R., 2015. Breakdown of the brain's functional network modularity with awareness. Proc. Natl. Acad. Sci. U. S. A. 112 (12), 3799–3804.
Greenberg, J.A., et al., 2015. Decreases in theta and increases in high frequency activity underlie associative memory encoding. Neuroimage 114, 257–263.
Gregoriou, G.G., et al., 2009. High-frequency, long-range coupling between prefrontal and visual cortex during attention. Science 324 (5931), 1207–1210.
Hamame, C.M., et al., 2014. High frequency gamma activity in the left hippocampus predicts visual object naming performance. Brain Lang. 135, 104–114.
Haque, R.U., et al., 2015. Cortical low-frequency power and progressive phase synchrony precede successful memory encoding. J. Neurosci. 35 (40), 13577–13586.
Howard, M.W., et al., 2003. Gamma oscillations correlate with working memory load in humans. Cerebr. Cortex 13 (12), 1369–1374.
Jerbi, K., et al., 2009. Task-related gamma-band dynamics from an intracerebral perspective: review and implications for surface EEG and MEG. Hum. Brain Mapp. 30 (6), 1758–1771.
Jones, M.W., Wilson, M.A., 2005. Theta rhythms coordinate hippocampal-prefrontal interactions in a spatial memory task. PLoS Biol. 3 (12), e402.
Kahana, M.J., 2006. The cognitive correlates of human brain oscillations. J. Neurosci. 26 (6), 1669–1672.
Kingyon, J., et al., 2015. High-gamma band fronto-temporal coherence as a measure of functional connectivity in speech motor control. Neuroscience 305, 15–25.
Kinnison, J., et al., 2012. Network analysis reveals increased integration during emotional and motivational processing. J. Neurosci. 32 (24), 8361–8372.
Kitzbichler, M.G., et al., 2011. Cognitive effort drives workspace configuration of human brain functional networks. J. Neurosci. 31 (22), 8259–8270.
Kucewicz, M.T., et al., 2014. High frequency oscillations are associated with cognitive processing in human recognition memory. Brain 137 (Pt 8), 2231–2244.
Lachaux, J.P., Rudrauf, D., Kahane, P., 2003. Intracranial EEG and human brain mapping. J. Physiol. Paris 97 (4–6), 613–628.
Lachaux, J.P., et al., 2012. High-frequency neural activity and human cognition: past, present and possible future of intracranial EEG research. Prog. Neurobiol. 98 (3), 279–301.
Liang, X., et al., 2016. Topologically reorganized connectivity architecture of default-mode, executive-control, and salience networks across working memory task loads. Cerebr. Cortex 26 (4), 1501–1511.
Mercier, M.R., et al., 2015. Neuro-oscillatory phase alignment drives speeded multisensory response times: an electro-corticographic investigation. J. Neurosci. 35 (22), 8546–8557.
Murray, R.J., Brosch, T., Sander, D., 2014. The functional profile of the human amygdala in affective processing: insights from intracranial recordings. Cortex 60, 10–33.
Musch, K., et al., 2014. Selective attention modulates high-frequency activity in the face-processing network. Cortex 60, 34–51.
Newman, M.E., 2006. Modularity and community structure in networks. Proc. Natl. Acad. Sci. U. S. A. 103 (23), 8577–8582.
Nir, Y., et al., 2008. Interhemispheric correlations of slow spontaneous neuronal fluctuations revealed in human sensory cortex. Nat. Neurosci. 11 (9), 1100–1108.
Ossandon, T., et al., 2012. Efficient pop-out visual search elicits sustained broadband gamma activity in the dorsal attention network. J. Neurosci. 32 (10), 3414–3421.
Palva, S., Monto, S., Palva, J.M., 2010. Graph properties of synchronized cortical networks during visual working memory maintenance. Neuroimage 49 (4), 3257–3268.
Perez, O., et al., 2015. Preconscious prediction of a driver's decision using intracranial recordings. J. Cogn. Neurosci. 27 (8), 1492–1502.

Power, J.D., et al., 2011. Functional network organization of the human brain. Neuron 72 (4), 665–678.
Price, C.J., 2000. The anatomy of language: contributions from functional neuroimaging. J. Anat. 197 (3), 335–359.
Roelfsema, P.R., et al., 1997. Visuomotor integration is associated with zero time-lag synchronization among cortical areas. Nature 385 (6612), 157–161.
Rubinov, M., Sporns, O., 2011. Weight-conserving characterization of complex functional brain networks. Neuroimage 56 (4), 2068–2079.
Sahin, N.T., et al., 2009. Sequential processing of lexical, grammatical, and phonological information within Broca's area. Science 326 (5951), 445–449.
Serletis, D., et al., 2014. The stereotactic approach for mapping epileptic networks: a prospective study of 200 patients. J. Neurosurg. 121 (5), 1239–1246.
Sperling, M.R., 1997. Clinical challenges in invasive monitoring in epilepsy surgery. Epilepsia 38 (4), S6–S12.
Sporns, O., 2010. Networks of the Brain. The MIT Press, p. 423.
Sporns, O., 2013. Network attributes for segregation and integration in the human brain. Curr. Opin. Neurobiol. 23 (2), 162–171.
Sporns, O., Betzel, R.F., 2016. Modular brain networks. Annu. Rev. Psychol. 67, 613–640.
Tononi, G., Sporns, O., Edelman, G.M., 1994. A measure for brain complexity: relating functional segregation and integration in the nervous system. Proc. Natl. Acad. Sci. U. S. A. 91 (11), 5033–5037.
Valencia, M., et al., 2008. Dynamic small-world behavior in functional brain networks unveiled by an event-related networks approach. Phys. Rev. E - Stat. Nonlinear Soft Matter Phys. 77 (5 Pt 1), 050905.
Vatansever, D., et al., 2015. Default mode dynamics for global functional integration. J. Neurosci. 35 (46), 15254–15262.
Wang, N., Zhang, L., Liu, G., 2015. EEG-based research on brain functional networks in cognition. Bio Med. Mater. Eng. 26 (1), S1107–S1114.
Wang, X., et al., 2016. The hierarchical structure of the face network revealed by its functional connectivity pattern. J. Neurosci. 36 (3), 890–900.
Winkler, A.M., et al., 2014. Permutation inference for the general linear model. Neuroimage 92, 381–397.
Womelsdorf, T., et al., 2006. Gamma-band synchronization in visual cortex predicts speed of change detection. Nature 439 (7077), 733–736.
Zheng, J., et al., 2017. Amygdala-hippocampal dynamics during salient information processing. Nat. Commun. 8, 14413.